

MEASUREMENT OF THE SPIN AND TEMPERATURE DEPENDENCE OF THE $dd\mu$ MOLECULE FORMATION RATE IN SOLID AND LIQUID DEUTERIUM

V.R. Bom**, J.D. Davies*, D. L. Demin, A. E. Drebusko, V. P. Dzhelepov, C. W. E. van Eijk**, V. V. Filchenkov, N. N. Grafov, V. G. Grebinnik, A. D. Konin, D. V. Migachev, A. I. Rudenko, V. T. Sidorov, Yu. G. Zhestkov, V. G. Zinov

Joint Institute for Nuclear Research
141980, Dubna, Russia

* University of Birmingham, Edgbaston, Birmingham B15 2TT, U.K.

** Delft University of Technology, NL-2629 JB, Delft, Netherlands

Submitted to 24 June 1996

The $dd\mu$ molecule formation rates have been measured from the two hyperfine states of the $d\mu$ atom in the temperature range of $T = 5-30$ K. Results are consistent with the measurement of the TRIUMF group at $T = 3$ K and contradict theoretical predictions. The work was performed on the JINR phasotron (Dubna).

1. INTRODUCTION

Muon Catalyzed Fusion (MCF) in pure deuterium (see scheme in Fig. 1) has relatively simple kinetics and therefore is an attractive way to check the basic principles of the theory of muonic molecule resonance formation. Recent years have provided significant success both in the theoretical consideration [1-3] and in the measurements [4-6] of the $dd\mu$ molecule formation rate ($\lambda_{dd\mu}$) including strong spin effects. As is seen from Fig. 2, measurements of the temperature dependence $\lambda_{dd\mu}(T)$ at $T > 20$ K are in excellent agreement with the «standard»

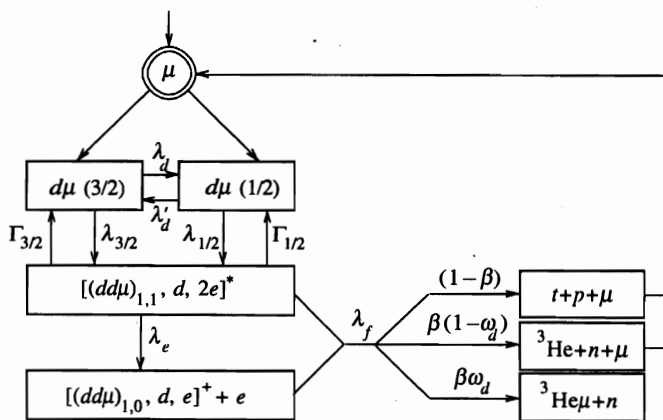


Fig. 1. Scheme of μ -catalyzed processes in pure deuterium

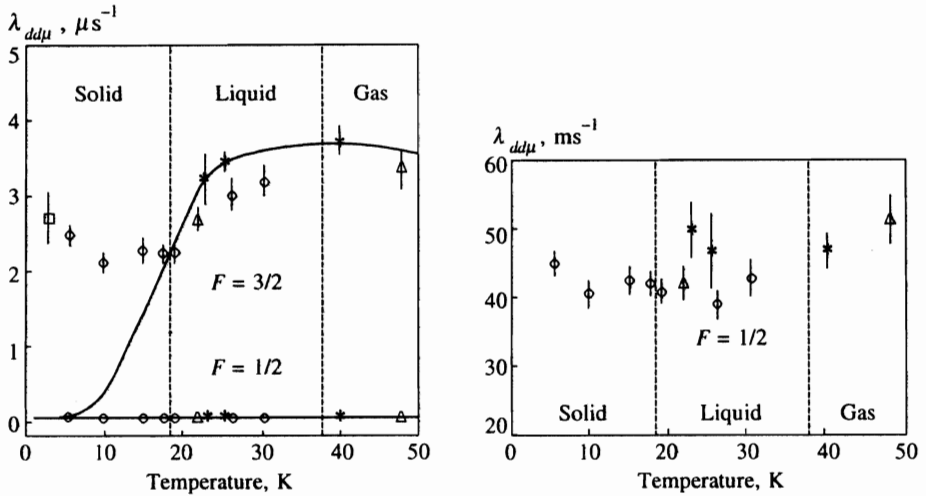


Fig. 2. Dependence $\lambda_{dd\mu}(T)$. Square — [7]; circles — present work; triangles — previous Dubna measurements [6]; stars — [4, 5]. The line corresponds to the «standard» theory [1–3]

theory of resonance muonic molecule formation. The most impressive consequence of their comparison is the determination of the energy of the weakly bound level in the $dd\mu$ system with an accuracy of ≈ 0.1 meV. Note that the latter corresponds to 1% of the relativistic contributions to this energy.

It was thought that measurements at lower temperatures would allow only improved accuracy of the main MCF parameters. However, the recent measurement of the $dd\mu$ molecule formation rate from the spin $F = 3/2$ state of the $d\mu$ atom at $T = 3$ K [7] shows a large discrepancy with theory. Our aim was to extend the systematic measurement of $dd\mu$ mesomolecule formation rate from the different hyperfine $d\mu$ atom states $\lambda_{3/2}$ and $\lambda_{1/2}$ and the hyperfine transition rate λ_d within the 5–30 K temperature range. Preliminary results have been published [8].

In this paper we give the results of full analysis including the determination of the absolute values of the resonant (from the $d\mu$ atom spin state $F = 3/2$) and nonresonant ($F = 1/2$) $dd\mu$ molecule formation rates. At low deuterium temperature these values were previously measured in liquid deuterium at $T = 22$ K [6] and $T = 23$ K [4] and showed a noticeable discrepancy with theory for the value of $\lambda_{1/2}$ (nonresonant) [9]. For normalization the authors of [7] used the value of $\lambda_{1/2}$ obtained in [4] and then corrected in [10]; they also were not able to measure the deuterium density directly in the experiment.

The important feature of the present is the measurements with liquid and solid deuterium were performed in the same experiment under conditions having well defined deuterium density and temperature.

2. EXPERIMENTAL METHOD

The experimental method has been detailed elsewhere [6]. We measured and analyzed the yield and time distribution of 2.5 MeV neutrons from the $d + d$ fusion reaction at seven temperatures in the range 5–30 K



A simplified schematic of the experimental apparatus is shown in Fig. 3. In particular a specially constructed solid deuterium target (T) of volume 280 cm^3 [11] and a total absorption neutron spectrometer [12] (NE-213 to provide $n - \gamma$ separation [13]). The spectrometer consisted of two identical parts symmetrically placed around the target with total volume of 22 liters. High neutron detection efficiency (solid angle $\simeq 65\%$ and intrinsic efficiency $\simeq 70\%$ resulted in sufficiently high counting rate yet relatively low random background.

The target was enclosed in a liquid helium cooling cryostat. Special attention was given to achieving a high uniformity in temperature and density throughout the large target volume. To this end, a heat conductor consisting of 500 copper wires 0.4 mm in diameter was set inside the target which produced temperature gradients throughout the target not higher than 0.1 K . Temperatures were measured by two helium thermometers which were placed at different heights inside the target whose temperatures were kept constant to within an accuracy of 0.2 K .

The deuterium was purified with a palladium filter down to 10^{-1} ppm impurity concentration. The protium content was no higher than 0.5% .

The trigger selected those events for further recording and analysis which corresponded to the appearance of the neutron $[4(N_1 + N_2)]$ and electron $[4(N_1 + N_2)]$ signals during the $10 \mu\text{s}$ gate, opened by the muon stop ($1 \cdot 2 \cdot 3 \cdot 4$) signal. Discrimination against backgrounds originating from the muon stops in the target walls places the requirement on electron times of $t_e > 0.2 \mu\text{s}$ after the muon stop ($t_0 = 0$).

As usual, the neutron yield was normalized to the number of electrons from the decay of muons stopped in deuterium. The time spectrum of μ -decay electrons obtained in the run at 19.0 K is shown in Fig. 4. It was analyzed using the expression

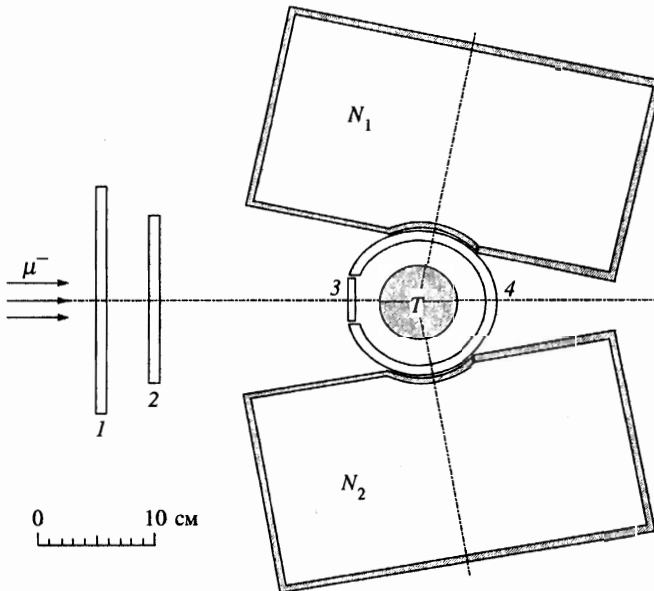


Fig. 3. Simplified scheme of the experimental setup. 1, 2, 3, 4 are scintillation counters; N_1, N_2 are total absorption neutron detectors, T is the deuterium target

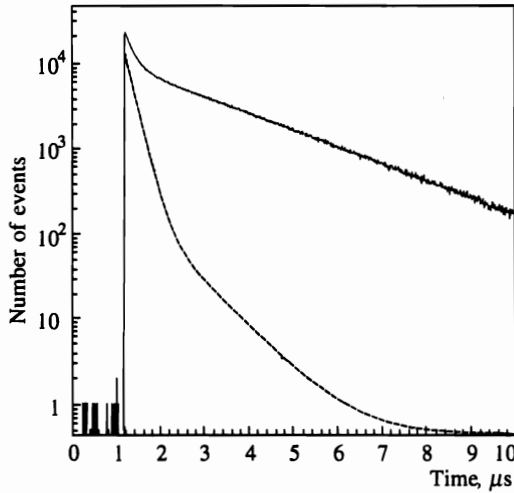


Fig. 4. Time spectrum of the decay electrons. The dashed line represents muon stops in the target walls

Table 1
Parameters of the exposures

Number	Target filling	Temperature, K	Density (LHD)	$N_e, 10^6$
1	Deuterium, solid	5.5(3)	1.43(4)	4.49(18)
2	—”—”—	9.9(2)	1.43(4)	2.983(14)
3	—”—”—	15.1(2)	1.42(4)	2.842(14)
4	—”—”—	17.7(2)	1.40(4)	5.777(19)
5	Deuterium, liquid	19.0(2)	1.31(4)	4.598(17)
6	—”—”—	26.3(3)	1.19(4)	2.786(13)
7	—”—”—	30.5(3)	1.08(4)	1.738(12)
8	Helium	14.7(2)	0.37(1)	1.487(9)
9	Vacuum			

$$N(t) = a_1 \exp(-\lambda t) + a_2 v(t) + a_3. \tag{2}$$

Here the short-lived component $a_2 v(t)$ (dashed curve in Fig. 4) represents muon stops in the target walls; its shape was determined from the measurements with an empty target. The slow exponent corresponds to muons stopped in deuterium with a slope very close to the free muon disappearance rate, ($\lambda_0 = 0.455 \mu s^{-1}$). The number of events belonging to the slow component (N_e) was used in analysis of the neutron events.

Experimental conditions for the 9 full runs are given in Table 1. As usual, the density is normalized relative to that of liquid hydrogen (LHD, $\phi_0 = 4.25 \cdot 10^{22}$ nuclei/cm³). The numbers in brackets represent uncertainties in the last figure(s).

The highest statistics were accumulated at the lowest temperature and in runs 4 and 5 which were as close as possible in temperature but in different deuterium phase states. The measurement with helium was made to determine independently the neutron background (a_3 in Eq. (2) above), while the data obtained with an empty target allowed us to check the number

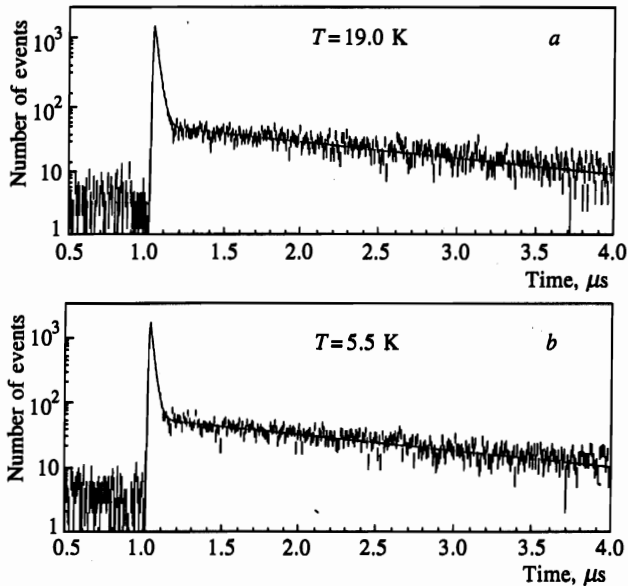


Fig. 5. Time spectra of the «first detected» catalysis neutron. The deuterium temperature: *a* — 19.0 K (liquid); *b* — 5.5 K (solid). Lines correspond to the function (4) with an optimal parameters found from the fit

of muon stops in the target walls.

Those events were selected for further analysis which satisfied the criteria of having:

- 1) A neutron in the $n - \gamma$ plot [6, 12].
- 2) A μ -decay electron in the time interval $t_n + 0.5 \mu\text{s} \leq t_e \leq t_n + 2.5 \mu\text{s}$.

Times and amplitudes (recoil proton energy) for those events were accumulated separately for each run and for each neutron detector. The final results were obtained from the analysis of such distributions for the «first detected» neutron events. However the high neutron detection efficiency allowed us to register the «second detected» fusion neutron; their yield and time distributions were then used to verify the normalization procedure and the detection efficiency calculation. Some neutrons time distributions are presented in Figs. 5*a, b* and 6. One can see that the relative yield of the background is low and that the neutron spectrum behavior remains the same when the temperature and the phase state of deuterium are changed.

3. KINETICS OF THE $d-d$ FUSION CYCLE

The scheme of the $d + d$ muon-catalyzed processes in pure deuterium is shown in Fig. 1. According to «standard» theory [1, 2] the $d\mu$ atoms are formed with an initial kinetic energy of a few electronvolts in two hyperfine states from which they are quickly thermalized. The thermalization rate is estimated to be $\lambda_{therm} \sim 10^9 \cdot \phi \text{ s}^{-1}$ [14, 15] which is much higher than the μ molecule formation and the spin-flip rates. The thermalization stage is therefore neglected in the «standard» theory.

Muonic molecules can be formed either via the nonresonant Auger process where the energy released under the $dd\mu$ formation is transferred to the conversion electron or via the Vesman

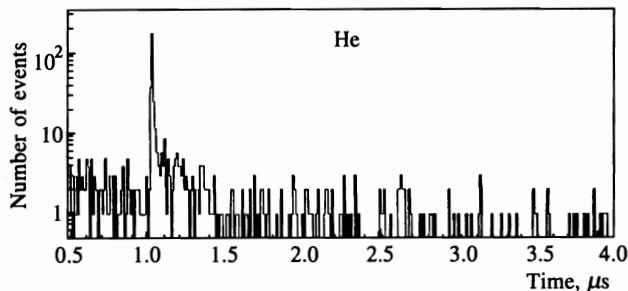


Fig. 6. Time spectrum of the background neutron events (target is filled with helium)

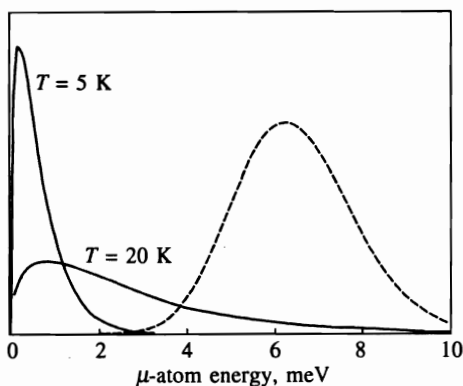


Fig. 7. Maxwell energy distribution of $d\mu$ atoms for $T = 5$ K and $T = 20$ K. The closest to zero resonance in the $dd\mu$ formation is shown by the dashed line

resonance mechanism [16]. The rate of nonresonant $dd\mu$ molecule formation depends slightly on the $d\mu$ atom energy ($\epsilon_{d\mu}$) and is equal to $0.03 - 0.04 \mu\text{s}^{-1}$ at $T \leq 50$ K [9]. According to the Vesman scheme, the resonant $dd\mu$ formation proceeds via the complex $[(dd\mu), d, 2e]^*$ which is in an excited state. This process is characterized by a set of resonances whose positions are determined by the spin states of the $d\mu$ atom ($F = 3/2, 1/2$) and of the $dd\mu$ molecules ($S = 3/2, 1/2$), as well as by the rotation states of the «initial» D_2 molecule (K_i) and the complex (K_f). The transitions having

$$F = 3/2 \longrightarrow S = 1/2, K_i = 0 \longrightarrow K_f = 1, K_i = 1 \longrightarrow K_f = 2 \quad (3)$$

dominate at the lowest temperatures [17].

Normally the $dd\mu$ formation is neglected during thermalization, but is considered for the Maxwell distributions of the $d\mu$ atom thermal energies. To obtain the values of $\lambda_{dd\mu}(T)$ for a given temperature, one therefore integrates the function $\lambda_{dd\mu}(\epsilon_{d\mu})$ [17] over the Maxwellian $W(\epsilon_{d\mu}; T)$. This procedure was used in [18] to give the dependence of $\lambda_{3/2}(T)$ presented in Fig. 2. The Maxwell distributions for $T = 5$ K and 20 K are shown in Fig. 7, together with the resonance closest in energy. As can be seen from this figure, the thermal energy distribution for $T = 5$ K does not overlap this resonance. Only the nonresonant $dd\mu$ formation is therefore expected to contribute at this temperature. From Fig. 7 it follows also that at $T = 20$ K $d\mu$ atoms spend a small part of their «Maxwell cycle» in the resonance region.

We conclude, that the measured value of $\lambda_{dd\mu}$ should therefore be compared with a calculated «effective» value which includes:

- 1) a contribution during the thermalization stage, no higher than a few percent [1, 2];
- 2) integration over the Maxwell distribution. Note that the competition between the spin-flip and scattering processes was not taken into account (see [18]);
- 3) only $\simeq 1/4$ part of the $dd\mu$ molecules undergoes fusion in competition with the back decay of the complex [1].

4. ANALYSIS

A set of the differential equations corresponds to the scheme of the $d-d$ fusion cycle shown in Fig. 1. When thermalization and the $d+d$ fusion rates are sufficiently high, it has an exact solution [1] which gives for the form of the neutron time distribution [1, 19]:

$$F_n(t) = b_f \exp(-\lambda_f t) + b_s \exp(-\lambda_s t). \quad (4)$$

For the fast exponent its slope λ_f is determined mainly by the spin-flip rate λ_d and its amplitude b_f is determined by the value of $\lambda_{3/2}$. The amplitude of the slow component b_s is close to the value of $\lambda_{1/2}$.

The parameters of the function (4) were found from the fit of the time distributions of the «first detected» neutrons. These spectra were convoluted with a Gaussian resolution function, to account for the finite time resolution (σ). The value of σ and the time zero (t_0) were optimized for each run. The analysis showed that the time zero stability during the data-taking was better than 1 ns. The background due to muon stops in the target walls was approximated by an exponent with the slope $\lambda_f^b = 5 \mu\text{s}^{-1}$. Accidental neutron events were fitted as an exponent with $\lambda_s^b = \lambda_0$ for $t_n \geq t_0$ and with a constant value for $t_n \leq t_0$.

At the next stage of the analysis the absolute values of the steady state $dd\mu$ -molecule formation rate were obtained from

$$\lambda_{ss} = \frac{\lambda_s}{\phi\beta_s} \left[\frac{N_n^s}{N_e} \epsilon_n f_t \right]. \quad (5)$$

Here the expression in the brackets means the absolute neutron yield for the steady state of the $d-d$ fusion cycle, λ_s is the slope of the «slow» exponent in (4) and β_s is the partial probability of the reaction (1). To a good approximation (better than 1%) $\beta_s = \beta_{nr} = 0.53$, where β_{nr} corresponds to the nonresonant $dd\mu$ formation.

In the expression for the absolute neutron yield N_n^s is the number of neutron events in the «slow» component of the time spectrum (4), N_e is the number of electrons indicated in Table 1, f_t allows for the finite time interval for detection of a fusion neutron followed by a μ -decay electron, and ϵ_n is the neutron detection efficiency. The latter was calculated using two «independent» Monte Carlo codes. One [20] was written specially for our experimental $d-d$ program and the other used the standard package GEANT [21] and the low-energy neutron cross sections therein. The results of the two codes coincide within 3–5%. To determine the efficiency loss due to the finite threshold the calculated recoil proton energy spectrum was reconciled with the experimental distribution. This procedure was repeated for data of each run and the example for $T = 19.0$ K is given in Fig. 8. The spikes in the spectrum are due to ADC differential nonlinearity.

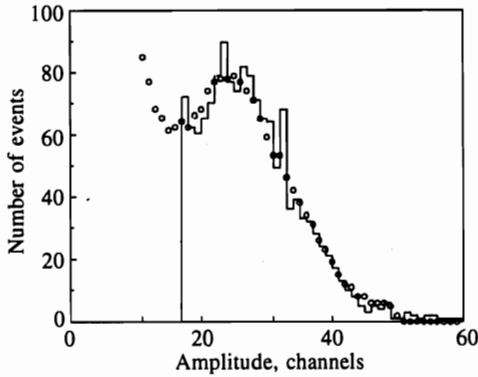


Fig. 8. Energy spectrum of protons recoiling from neutrons plotted for detector N1 with the target at 19.0 K (histogram). Circles are the corresponding calculations. The number of events is given in arbitrary units

The value of λ_{ss} , as well as the slope λ_s and the ratio b_f/b_s (4), are found from the fit used for the numerical solution of the set of differential equations referred to above. For the partial probability of the reaction (1) $\beta_r = 0.58$ was used for the resonant $dd\mu$ formation ($F = 3/2$) and $\beta_{nr} = 0.53$ was used for the nonresonant formation ($F = 1/2$) [22]. This procedure then gave the values of $\lambda_{3/2}$, $\lambda_{1/2}$, and λ_d . There were a few small corrections (few percent), e.g., for the loss due to $n - \gamma$ separation.

5. RESULTS AND DISCUSSION

The experimental results are presented in Table 2.

Table 2

Experimental results

Temperature, K	The rates of the $dd\mu$ molecule formation and $d\mu$ atom hyperfine transition rate, μs^{-1}			
	$\lambda_{1/2}$	$\lambda_{3/2}$	$\lambda_{3/2}/\lambda_{1/2}$	λ_d
5.5	0.0448(18)	2.48(13)	55.3(1.8)	31.7(1.0)
9.9	0.0403(20)	2.11(14)	52.3(2.3)	29.3(1.2)
15.1	0.0424(20)	2.27(16)	53.5(2.4)	32.5(1.5)
17.7	0.0419(18)	2.24(11)	53.4(1.7)	32.8(1.2)
19.0	0.0407(21)	2.27(14)	55.8(1.9)	30.2(1.0)
26.3	0.0389(20)	3.03(20)	77.8(2.4)	36.1(1.4)
30.5	0.0428(26)	3.20(21)	74.8(2.4)	32.0(1.1)

The values in brackets are the errors due only to statistics, the fit and the corrections and do not include systematic uncertainties from ϕ (3%) and ϵ_n (8%). Our results are shown in Figs. 2 and 9, together with the data of other authors. Again, our data are given without systematic errors in order to show more clearly their dependence on temperature.

The data for the «second detected» neutrons ($N_1 - N_2$ and $N_2 - N_1$) were also analyzed. Their time distribution relative to the «first detected» neutrons is shown in Fig. 10. The data are summed over all exposures with solid deuterium. The curve in this figure corresponds to

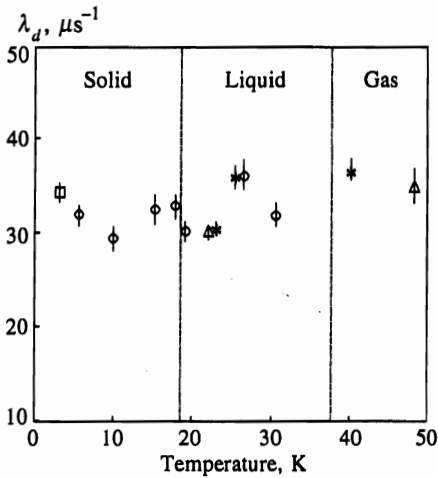


Fig. 9. Experimental data on the $d\mu$ atom spin-flip rate, λ_d . Square — [7]; circles — present work; triangles — previous Dubna measurements [6]; stars — [4, 5]

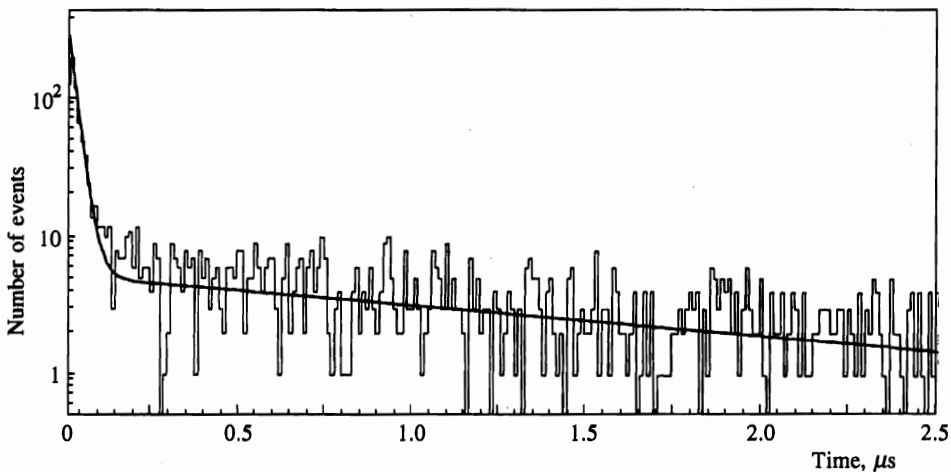


Fig. 10. Time distribution of the «second detected» neutron accumulated for all exposures with solid deuterium. Line is the function (4) with the exponent slopes obtained from the analysis of the «first detected neutrons»

exponents with the «fast» and «slow» slopes found above in the analysis of the «first» neutrons. The measured and the predicted spectra are in satisfactory agreement.

The value of $\lambda_{1/2}^{(2)}$ was found from the analysis of the «second» neutrons normalized to the number of «first» neutrons:

$$\lambda_{1/2}^{(2)} = 0.041(3) \mu s^{-1} \quad (\text{statistical error only}).$$

This value agrees with that obtained for the «first» neutrons.

As can be seen from Fig. 2 our data for $\lambda_{1/2}$ are in agreement both with our previous measurement with liquid deuterium at $T = 22$ K and with the results of the PSI group at $T = 23$ K; the latter initially gave $\lambda_{1/2} = 0.0500(34)(22) \mu s^{-1}$ [4] and then in [10] as $\lambda_{1/2} =$

$= 0.045(5)\mu\text{s}^{-1}$. Also the experimental results are in excess of theoretical prediction, $\lambda_{1/2}^{(th)} \sim \sim 0.03\mu\text{s}^{-1}$ [9].

Of course, our main result is the measurements of the $dd\mu$ molecule formation rate from the upper $d\mu$ atom spin state for the lowest deuterium temperatures. Together with the pioneering result of the TRIUMF group [7] they sharply contradict the «standard» theory, according to which only the nonresonant $dd\mu$ formation from the $d\mu$ atom spin states can contribute at the lowest temperatures. Possible mechanisms to explain it are considered in [18, 22, 23].

According to [22] the $d\mu$ atoms moving in solid deuterium have insufficient time to fully thermalize, because they lose energy only in inelastic interactions with the lattice excitation. Significant $dd\mu$ formation therefore, occurs at energies higher than thermal. This effect can explain the experimental data qualitatively [18] but quantitative agreement with the experiment is achieved only for few definite values of the inelastic cross sections. This mechanism could be investigated by repeating the experiment with enhanced protium.

Another possible explanation involves transitions with negative $d\mu$ atom resonance energy for $dd\mu$ formation [23] with the transfer of the released energy to lattice excitation. The transition $K_i = 1 \rightarrow K_f = 0$ is appropriate for this scheme. The liquid and solid deuterium in this experiment were held at the room temperature ortho-para ratio because equilibration is so slow. The experiment should be repeated with catalyzed $p \rightarrow \sigma$ to, inter alia, check this mechanism because with pure ortho-deuterium [23] only transitions with positive resonance energies are possible (3).

Of course, both mechanisms can explain the experimental results, but, as was pointed out in [18], the data for solid and liquid deuterium are practically identical. Perhaps the problem is more complicated and needs a more complete consideration. Incidentally the enhanced rate is independent of the structure of the solid deuterium lattice viz the TRIUMF group formed fcc solid deuterium directly from the gas phase, whereas our solid deuterium had hcp structure as it came from the liquid.

Finally, the experimental data on λ_d are given in Fig. 9. Our results are in agreement with the previous measurements, both in the solid and liquid deuterium. At the same time, full set of the data for $T \leq 30$ K does not show such a sharp difference from the results for gaseous deuterium as was manifested for the first measurement in liquid deuterium.

We wish to thank E. P. Krasnoperov for developing the solid-deuterium target. We also thank M. M. Petrovsky' and A. P. Kustov for help in tests and runs.

The work was performed under the assistance of the Russian Foundation for Basic Research and INTAS (Brussels).

References

1. L. I. Menshikov, L. I. Ponomarev, T. A. Strizh, and M. P. Faifman, Zh. Exp. Theor. Phys. **92**, 1173 (1987), Sov. Phys. JETP **65**, 656 (1987).
2. M. P. Faifman, Muon Cat. Fusion **2**, 247 (1988). M. P. Faifman, L. I. Menshikov, and T. A. Strizh, Muon Cat. Fusion **4**, 1 (1989).
3. A. Scrinzi, Muon Cat. Fusion **5/6**, 179 (1990).
4. N. Nagele, W. H. Breunlich, M. Cargnelli et al., Nucl. Phys. A **493**, 397 (1989).
5. J. Zmeskal, W. H. Breunlich, M. Cargnelli et al., Muon Cat. Fusion **1**, 109 (1987). W. H. Breunlich, M. Cargnelli, P. Kammel et al., Muon Cat. Fusion **5/6**, 149 (1987).

6. V. P. Dzheleпов, V. G. Zinov, S. A. Ivanovsky' et al., Zh. Exp. Teor. Phys. **101**, 1105 (1992); Sov. Phys. JETP **74**, 589 (1992); Muon Cat. Fusion **7**, 387 (1992).
7. P. Kammel, in *Muonic Atoms and Molecules, Proc. of the Int. Workshop at the Centro Stefano Franchini on Monte Verita*, ed. by L. Schaller, C. Petitjean, Birkhauser Verlag, CH-4010, Basel, Boston, Berlin (1993), p. 111. P. E. Knowles, J. M. Bailey, G. A. Beer et al., Hyp. Int. **101/102**, 21 (1996).
8. D. L. Demin, V. P. Dzheleпов, V. V. Filchenkov et al., Hyp. Int. **101/102**, 13 (1996).
9. M. P. Faifman, Muon Cat. Fusion **4**, 341 (1989).
10. A. Scrinzi, P. Kammel, J. Zmeskal et al., Phys. Rev. A **47**, 4691 (1993).
11. D. L. Demin, V. P. Dzheleпов, N. N. Grafov et al., Hyp. Int. **101/102**, 583 (1996).
12. V. P. Dzheleпов, V. V. Filchenkov, A. D. Konin et al., Nucl. Instr. and Meth. A **269**, 634 (1988).
13. V. G. Zinov, E. Lonsky, and A. I. Rudenko, Prib. Tech. Exp. № 1, 91 (1991).
14. A. Adamchak and V. S. Melezhik, Muon Cat. Fusion **5/6**, 303 (1990).
15. J. B. Kraiman, W. H. Breunlich, M. Cagnelli et al., Muon Cat. Fusion **5/6**, 43 (1990), Phys. Rev. Lett. **63**, 1942 (1989).
16. E. A. Vesman, Pis'ma Zh. Exp. Teor. Phys. **5**, 113 (1967), Sov. Phys. JETP Letters **5**, 91 (1967).
17. M. P. Faifman, T. A. Strizh, E. A. G. Armour et al., Hyp. Int. **101/102**, 179 (1996).
18. V. V. Filchenkov, Hyp. Int. **101/102**, 37 (1996).
19. V. V. Filchenkov, Communications JINR E1-89-57, Dubna (1989).
20. V. V. Filchenkov and L. Marczis, Communications JINR E13-88-56, Dubna (1988).
21. CERN Program Library, W5013.
22. A. Adamchak, Hyp. Int. **101/102**, 113 (1996).
23. L. I. Menshikov and V. V. Filchenkov, Hyp. Int. **101/102**, 207 (1996).